Intraplane to interplane optical interconnects using LiNbO3-based electrooptically modulated switch array for high density holographic memory

De-Gui Sun, Chunhe Zhao, and Ray T. Chen

Mricoelectronics Research Center
Department of Electrical and Computer Engineering
The University of Texas at Austin
Austin, Texas 78712-1084

ABSTRACT

A new optical interconnect architecture for a three-dimensional switch array using multiple $LiNbO_3$-based electro-optically modulated gratings in conjunction with substrate guided waves is reported. First the operating mechanism of the system is studied in detail, and the momentum mismatch in the operating process of the system is also demonstrated. Then, a new method for calculating coupling efficiency is derived by introducing a compensation for the mismatch. With the new calculation method and by introducing a substrate guided wave with 45° bouncing angle and 100-V applied voltage, an optimized coupling efficiency is obtained even though it is under the case of momentum-mismatch. Finally, the experimental result of coupling efficiency of the electrooptically modulated grating is provided, and agreements between the experimental results and the theoretical prediction are obtained.

Keywords: High density memory, angle-multiplexing, optical interconnection, electro-optic grating, momentum-mismatch, phase compensation, coupling efficiency.

1. INTRODUCTION

High capacity programmable holographic memories without any moving part have long been considered as a feasible solution to upgrade the memory density and the access time[1-3]. Multiplexibility of holographic medium plays an important role in realizing high density holographic memories[2,3]. Many new optical interconnect technologies such as holographic gratings, phase gratings, waveguide couplers, microlens arrays, fibers, vertical-cavity surface emitting laser (VCSEL) arrays and photodetector arrays are approaching commercial levels[4-10]. In particular, the reconfigurable optoelectronic interconnects have received more attention because they are more suitable for the above optical information processing areas[4-6]. One of the most pivotal elements for the realization of these applications is electrooptic (EO) modulated phase grating that has been used to perform switching, numerical operations and interconnections for computing and information processing[7-10].

However, the study of EO grating with high diffraction efficiency and short interaction length has not been investigated carefully because of the fact the momentum match for high diffraction efficiency based on the Bragg diffraction theory is not easy to realize[11]. In this paper, we investigate a microstructure electrooptic grating based on the $LiNbO_3$ crystal for a novel intraplane to interplane interconnect application. Substrate guided waves are employed to provide the signal, which may be data, image, etc. The momentum mismatch is verified in the operating process of the system. A new method for calculating coupling efficiencies by introducing a compensation for the mismatch is proposed and an

SPIE Vol. 3005 • 0277-786X/97/$10.00

optimized architecture is obtained. Therefore the result presented herein provides not only a higher design accuracy, but also a high coupling efficiency.

2. PROPOSED CONFIGURATION FOR HOLOGRAPHIC RECORDING AND READING

The proposed configuration for successively recording and reading holograms are depicted in Figs. 1(a) and 1(b), respectively. In this system, the guided-wave-interconnects based on an one-dimensional $LiNbO_3$-based EO grating array containing 30 individually addressable EO gratings are employed to introduce the reference beam through total internal reflections (TIRs) with a pre-determined bouncing angle, and free-space interconnects are used to introduce the object beam.

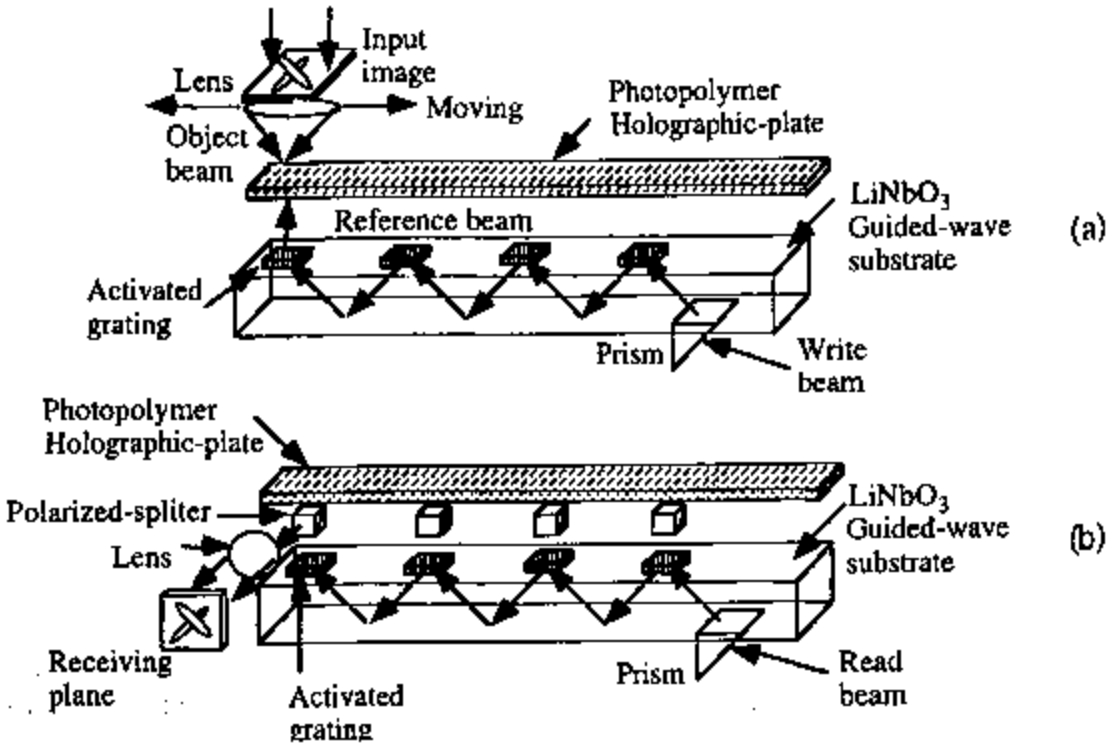

Fig. 1 Proposed configuration for successive holographic recording and reading: (a) schematic for recording data; and (b) schematic for reading data.

3. DETERMINATION OF THE BOUNCING ANGLE IN $LiNbO_3$

The purpose of this research is to study and design an EO grating with a short interaction length as shown in Fig. 2. $LiNbO_3$ is used to produce index modulation by the use of microelectrodes at various spots marked with G_i, while polymer is used to fulfill such required functions as wavelength redistribution and data storage and reading.

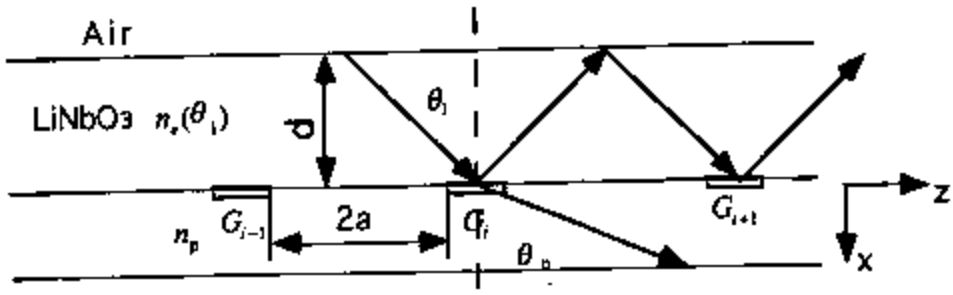

Fig. 2 Construction of $LiNbO_3$-based electrooptic diffraction grating.

When the EO grating is activated, the optical beams are coupled with the high efficiency into the polymeric material when an appropriate voltage is applied. Otherwise the beams are total-internally reflected at these spots when the associated electrooptic grating is not activated. This operating process is shown schematically in Fig. 3 in which the coupling process is performed between the first layer and the second layer. The second layer functions as the index modulation layer of grating, and its thickness L_e is the effective modulation depth of $LiNbO_3$ crystal. Of course the second layer does not exist when the EO grating is not activated and the bouncing process is performed between the first layer and the third layer. Therefore the first requirement is achieved by a bouncing angle θ_1 in $LiNbO_3$ that is bigger than the critical angle θ_c, and the second requirement is achieved by a diffraction angle θ_2 in the second layer of $LiNbO_3$ that is smaller than the critical angle θ_c. Therefore the bouncing beam within the $LiNbO_3$ substrate can be controlled to be out by the given activated EO grating.

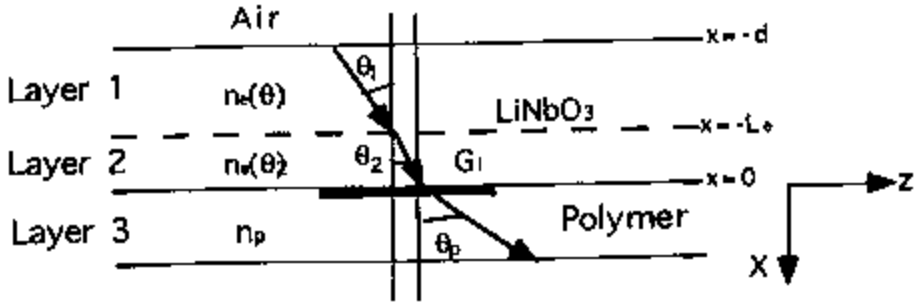

Fig. 3 Relationships among the unmodulated $LiNbO_3$ layer (1), the modulated layer (2), and the photopolymer memory layer (3).

4. THE ELECTRIC FIELD DISTRIBUTION

As illustrated in Fig. 2, the electrodes are fabricated along the z axis and the light wave travels within the z-x plane. When voltage V is applied across the electrodes and if the width of the spacing between the electrodes is 2a, we have

$$\frac{\partial^2 V}{\partial z^2}+\frac{\partial^2 V}{\partial x^2}=0 \quad (x>0) \tag{1a}$$

$$\varepsilon_z \frac{\partial^2 V}{\partial z^2} + \varepsilon_x \frac{\partial^2 V}{\partial x^2} = 0 \quad (-d \le x \le 0) \tag{1b}$$

where ε_z and ε_x are dielectric constants in direction z and x, repectively. By our using the coordinate transformation

$$x' = \sqrt{\varepsilon_z / \varepsilon_x}\, x \tag{2}$$

Eq. (1b) can also be written as:

$$\frac{\partial^2 V}{\partial z^2} + \frac{\partial^2 V}{\partial x'^2} = 0 \tag{3}$$

By using the coordinate transformation as follows again:

$$z = a \cosh u \cos v \tag{4a}$$

$$x' = a \sinh u \sin v \tag{4b}$$

the resolutions for Eq. (3) can be written as: [12]

$$E_z = -\left(\frac{V}{a\pi}\right) \frac{\cosh u \sin v}{\cosh^2 u - \cos^2 v} \tag{5a}$$

$$E_x = -\left(\frac{V}{a\pi}\right) \frac{\sinh u \cos v}{\cosh^2 - \cos^2 v} \sqrt{\varepsilon_x / \varepsilon_z} \tag{5b}$$

Therefore, Eqs. (4) and (5) determine the distribution of electric field components in directions z and x. Furthermore, in accordence with the crystal optics principle[11], we can study the index modulation of $LiNbO_3$ induced by the electric field as follows:

$$\Delta n_e(\theta_1) = \frac{n_e^3 \sin^2 \theta_1 \Delta n_o + n_o^3 \cos^2 \theta_1 \Delta n_e}{(n_o^2 \cos^2 \theta_1 + n_e^2 \sin^2 \theta_1)^{3/2}} \tag{6}$$

where Δn_e and Δn_o are calculated by

$$\Delta n_e = -\frac{1}{2} n_e^3 r_{33} E_z \tag{7a}$$

$$\Delta n_o = -\frac{1}{2} n_o^3 r_{13} E_z \tag{7b}$$

where γ_{33} and γ_{13} are the EO coefficients of $LiNbO_3$ gratings.

5. COUPLING CONDITIONS AND MOMENTUM-MISMATCH OF SYSTEM

In this system, the coupling of optical beams under the action of the EO grating is a key operation. Because some factors supporting the operation, such as the grating direction and period, the directions and amplitudes of wave vectors, and the index modulation of the $LiNbO_3$ crystal, are all limited by the system itself, coupling conditions and efficiency are worthy of the detailed study. As shown in Fig. 4, K_1, K_2, and K_g indicate the incident wave vector, the diffracted wave vector, and the grating vector, respectively.

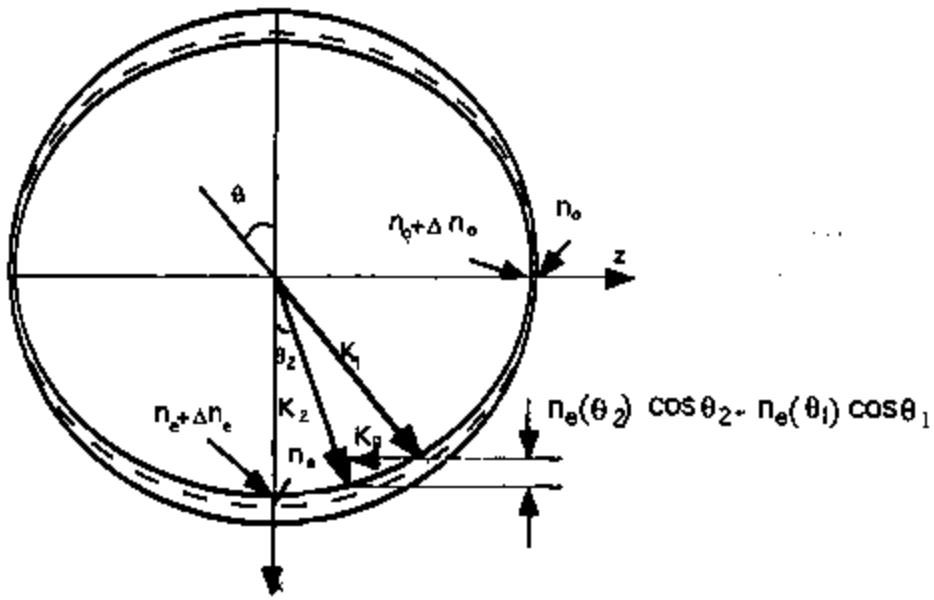

Fig. 4 Wavevectors and modulation scheme of an x-cut $LiNbO_3$ crystal.

In z direction, we define

$$\beta_1 = \frac{2\pi}{\lambda} n_e(\theta_1)\sin\theta_1 \tag{8a}$$

$$\beta_2 = \frac{2\pi}{\lambda} n_e(\theta_2)\sin\theta_2 \tag{8b}$$

$$k_g = \frac{2\pi}{\Lambda} \tag{8c}$$

In x direction, we define

$$\alpha_1 = \frac{2\pi}{\lambda} n_e(\theta_1)\cos\theta_1 \tag{9a}$$

$$\alpha_2 = \frac{2\pi}{\lambda} n_e(\theta_2)\cos\theta_2 \tag{9b}$$

where λ and Λ are the wavelength and the grating period, respectively. Based on the above equations, the momentum mismatches in both z and x directions are defined as follows:

$$\Delta\beta = \beta_1 - \beta_2 - mk_g \tag{10}$$

$$\Delta\alpha = \alpha_2 - \alpha_1 \tag{11}$$

In the Bragg diffraction theory, the vectors that are only in the grating direction are required to be matched, i.e., $\Delta\beta = 0$[11]. It is certain that the value of $[n_e(\theta_2)\cos\theta_2 - n_e(\theta_1)\cos\theta_1]$ functions as the grating period Λ or diffraction angle θ_2. In terms of Bragg diffraction theory, if both $\Delta\beta$ and $\Delta\alpha$ are zero, three vectors, K_1, K_2, and K_g are matched, which is the perfect Bragg diffraction, and the diffraction efficiency of 100% can be realized theoretically. Then with Eqs. (9a), (9b) and (11), we obtain the distribution curves of $\Delta\alpha\lambda / 2\pi = [n_e(\theta_2)\cos\theta_2 - n_e(\theta_1)\cos\theta_1]$ with diffraction angle θ_2, as shown in Fig. 5.

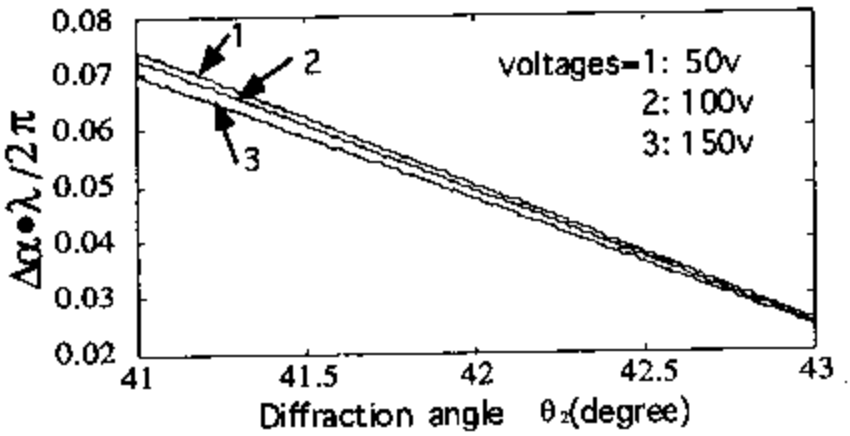

Fig. 5 Relationship between $\Delta\alpha \bullet \lambda / 2\pi$ and diffraction angle.

Note that $\Delta\alpha\lambda / 2\pi = [n_e(\theta_2)\cos\theta_2 - n_e(\theta_2)\cos\theta_1]$ is always larger than 0, which means that the matching condition defined by Eqs. (10) and (11) among the three vectors K_1, K_2, and K_g, does not exist at all. However, $\Delta\alpha$ is an important factor in influencing the coupling efficiency in accordance with the Bragg diffraction theory. A bigger $\Delta\alpha$ can induce the multimode coupling, so we have to study the multimode extension of grating coupling from the compensation for the momentum mismatch $\Delta\alpha$.

6. COMPENSATION FOR MISMATCH AND OPTIMIZATION FOR COUPLING EFFICIENCY

Assuming $A_1(x)$ and $A_2(x)$ are the components of the complex amplitudes of the normalized modes of incident light wave and diffracted light wave in x direction, we have[11]

$$\frac{dA_1(x)}{dx} = -ik_{12}A_2(x)e^{i\Delta\alpha x} \tag{12a}$$

$$\frac{dA_2(x)}{dx} = -ik_{12}^{*}A_1(x)e^{-i\Delta\alpha x}, \text{ and} \tag{12b}$$

$$k_{12} = \frac{\omega^2\mu}{2\sqrt{\alpha_1\alpha_2}}P_1 \bullet \Delta\varepsilon P_2 \tag{12c}$$

where k_{12} is coupling constant, $\omega = 2\pi c/\lambda$ is angular frequency, P_1 and P_2 are unit vectors in the incident wave and the diffracted wave directions, μ is the permeability of $LiNbO_3$, and $\Delta\varepsilon$ is the increment of dielectric constant ε. With Eq. (1) and optical principle, we can obtain the increment of dielectric constant as

$$\Delta\varepsilon = 2\varepsilon_o n_o n_e \frac{n_o^3\cos^3\theta_1\Delta n_e + n_e^3\sin^3\theta_1\Delta n_o}{(n_e^2\sin^2\theta_1 + n_o^2\cos^2\theta_1)^2} \tag{13}$$

Note that here we are discussing the codirectional coupling. The coupled mode Eqs. (12a) and (12b) are consistent with the energy conservation in x direction, i.e.,

$$\frac{d}{dx}\{|A_1|^2 + |A_2|^2\} = 0 \tag{14}$$

When $\Delta\alpha$ is large, Eq. (14) cannot be satisfied, and the set of coupling Eqs. (12a), (12b) and (12c) is no longer valid, and the mode extension has to be used to analyze the coupling procedure of grating. In terms of the mode expansion principle, the TE modes of the diffracted optical waves in the region $x \geq 0$ is represented by the sum of the normal modes as[13, 14]

$$A_2(x) = \sum_{m=-\infty}^{\infty} e^{-i\Delta\alpha x}f_{m2}(z) \tag{15}$$

where

$$f_{m2}(z) = h_{m2}(z) / \sqrt{D_{m2}}, \text{ and} \tag{16a}$$

$$D_{m2} = \int_0^{\Lambda} |h_{m2}(z)|^2 dz, \text{ and} \tag{16b}$$

$$h_{m2}(z) = \Delta n_e(\theta_1, x)e^{-i\beta_{1z}} \tag{16c}$$

As shown in Fig. 6(a), the diffracted wave represented by Eq. (15) produces an interaction with grating in the region of interaction depth from $-L_e$ to 0. The interaction depth has its inherent spatial frequency spectrum that covers all the diffraction modes and functions as a phase compensation region before the diffracted wave forms all the possible modes. As a phase compensation, this frequency spectrum can be calculated by

$$A_2(\Delta r) = \int_{-L_e/2}^{L_e/2} f_{m2}(z) e^{-i\Delta r x} dx \qquad (17)$$

where Δr is the spetial angular frequency in x direction. Then for the energy of diffracted wave, we obtain the transmittance spectrum of the interaction depth as

$$\tau(\Delta r) = [\frac{\sin(L_e \Delta r)}{L_e \Delta r}]^2 \qquad (18)$$

The transmittance spectrum curve is shown in Fig. 6(b). The coupling efficiency of the EO modulation grating can be calculated in accordance with Fig. 6(b), which depends on the compensation of Δr for the mismatch $\Delta\alpha$. For example, when the grating period $\Lambda = 8\mu m$, we obtain $\Delta\alpha \approx 0.6 \times 10^6$ by Eq. (11). As shown in Fig. 6(b), transmittance value is approximately 44%.

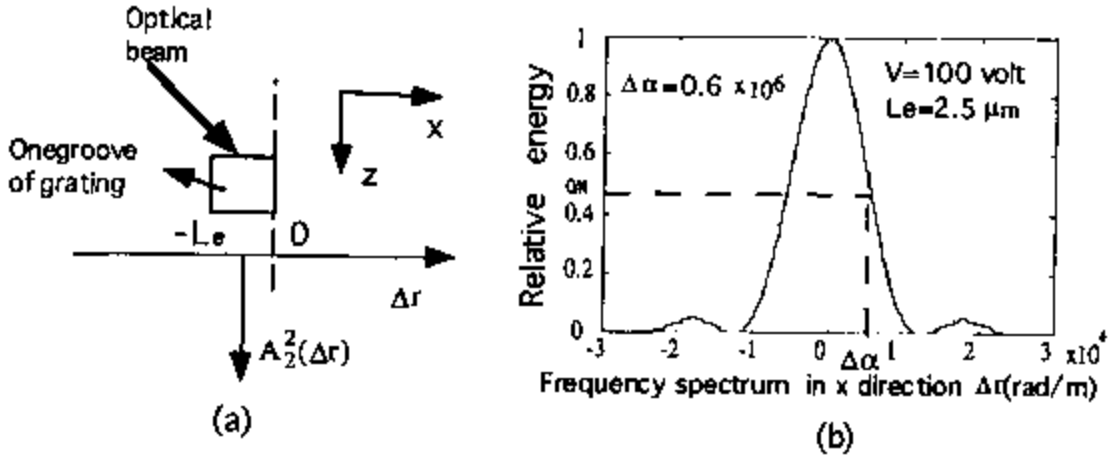

Fig. 6 Frequency spectrum of grating depth: (a) diffraction theorem; and (b) spatial frequency spectrum.

By considering the phase compensation for the mismatch $\Delta\alpha$, one can change the set of coupling equations (12a) and (12b) to

$$\frac{dA_1(x)}{dx} = -ik_{12}A_2(x) \qquad (19a)$$

$$\frac{dA_2(x)}{dx} = -ik_{12}^{*}A_1(x) \tag{19}$$

Finally, we obtaion the coupling efficiency of grating as:

$$\eta = [\frac{\sin(L_e\Delta\alpha)}{L_e\Delta\alpha}]^2 \cdot \sin^2(k_{12} \cdot L_e) \tag{20}$$

As we know, Le depends on the applied voltage and index modulation $\Delta n_e(\theta_1)$ which again is ... by the applied voltage. Because both the interaction length Le and the index modulation $\Delta n_e(\theta_1)$ ... on the applied voltage, and k_{12} functions as both the index modulation $\Delta n_e(\theta_1)$ and the diffracti... θ_2, we must optimize the coupling efficiency by taking account the total effectivity of all the ... parameters as follows:

$$k_{12} = \frac{4\pi^2 n_o n_e}{\lambda^2\sqrt{\alpha_1\alpha_2}} \cdot \frac{n_o^3\cos^3\theta_1\Delta n_e + n_e^3\sin^3\theta_1\Delta n_o}{(n_e^2\sin^2\theta_1 + n_o^2\cos^2\theta_1)^2}\cos(\theta_1 - \theta_2) \tag{21}$$

$$k_{12}L_e = \int_{-L_e}^{0} k_{12}dx \tag{22}$$

$$\int_{-L_e}^{0} k_{12}dx = \frac{4\pi^2 n_o^4 n_e^4\cos(\theta_1 - \theta_2)}{\lambda^2(n_e^2\sin^2\theta_1 + n_o^2\cos^2\theta_1)^2\sqrt{\alpha_1\alpha_2}}(r_{33}\cos^3\theta_1 + r_{13}\sin^3\theta_1)\int_{-L_e}^{0} E_z dx \tag{24}$$

With Eqs. (20)-(23), we obtain the coupling efficiency curve as shown in Fig. 7. We can find from the figure that, when Λ equals approximately 8μm (as we selected in our project), the coupling efficiency is approximately 18%. In this simulation, we use the applied voltage of 100-V.

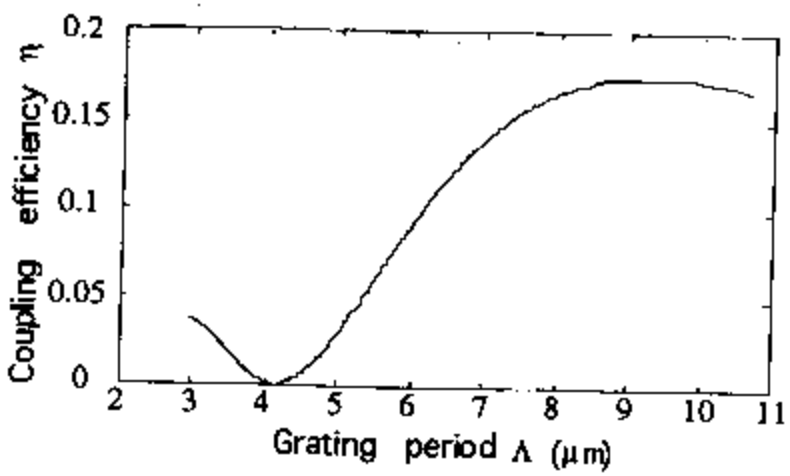

Fig. 7 Coupling efficiency of the EO grating as a function of grating period.

The fabricated $LiNbO_3$ EO grating array is shown in Fig. 8 where a linear EO grating array with the associated elements is clearly shown, where 30 independently addressable EO gratings are made on a $LiNbO_3$ substrate. The width of an electrode is 2μm and the spacing between two electrodes is 6μm, the period of the EO grating is 8μm. The observed fanout and the measured values of various diffraction orders corresponding to the above-mentioned experimental setting are illustrated in Figs. 9(a) and 9(b), respectively. Note that these diffraction orders can be selected as reference beams to record holograms in different recording angles. Hence, based on the interconnect architecture, the angularly multiplexed holographic recording and reading can be implemented on the same spot without any moving part.

Fig. 8. Picture of a real device, where 30 independently addressable EO gratings are made on the $LiNbO_3$ substrate.

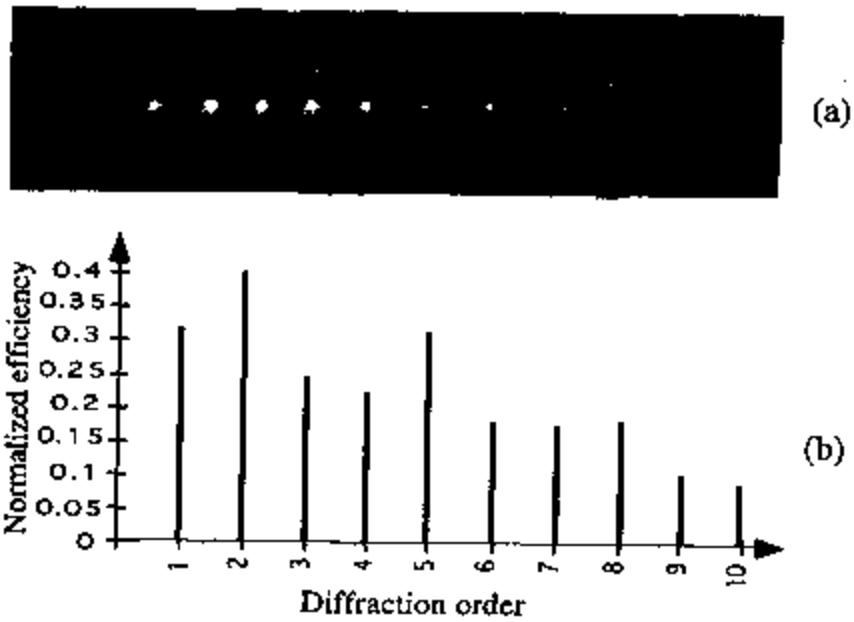

Fig. 9 The observed fanout of various diffraction orders of the EO grating: (a) diffraction orders; and (b) the coresponding measured values.

2. THE EXPERIMENTS OF EO GRATING MODULATION AND HOLOGRAPHIC MEMORY

The experimental setup for an AC measurement is shown in Fig. 10(a), where a AC voltage, a highly sensitive detector and an oscilloscope are used. A pair of test-probe positioners are used to effectively apply the modulation voltage onto the EO gratings. The experimental result of the EO modulated grating coupling is shown in Fig. 10(b) which represents $14 \pm 2.5\%$ coupling efficiency at 100 volts.

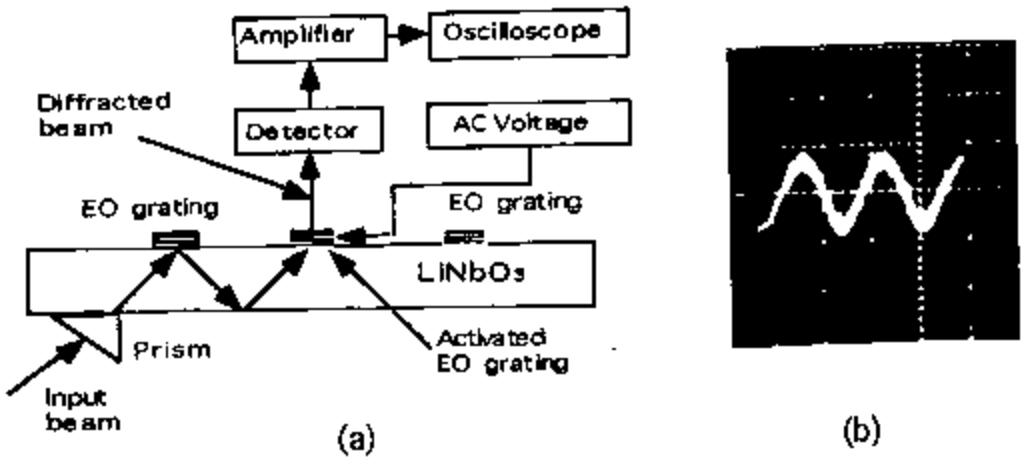

Fig. 10 Experiments of the coupling efficiency measurment of EO grating: (a) the setup; and (b) modualtion transfer curve of coupling efficiency, which represents 14 ±2.5% (f=60Hz)

In the experiment of the holographic write/read, a Fourier transform lens with the f/# of 2.0 is used. The size of input image of a bird pattern as shown in Fig. 11(a) is $7.68\times7.68\text{mm}^2$, which contains 256×256 bits defined by a liquid crystal display. We obtain two reconstructed images at $\lambda = 0.633\mu\text{m}$. Figure 11(b) shows the reconstructed image recorded at 30° angle, while Figure 11(c) is recorded at 60°. The so-called recording angle is the angle between the object beam and reference beam. Note that these two reconstructed images have different qualities because they are recorded at two different write angles.

Fig. 11 Experiments of holographic memory: (a) the input image; (b) the reconstracted image obtained at 30° recording angle; and (c) the reconstructed image obtained at 60° recording angle.

8. SUMMARY AND CONCLUSION

We present the theory in the design of a new microstructural high diffraction efficiency EO grating using substrate guided waves. In this research, the operating mechanism under momentum mismatch of the system is explained with a new coupling theory, and the coupling efficiency is calculated in the modified formula. In addition, the relation between the periodicity and the diffraction angle is delineated, and the relationship of the grating period of the EO grating and momentum mismatch in the vertical direction $\Delta\alpha$ is discussed. The most important aspect in the research is a new conclusion that a grating coupler requires only the momentum match in the direction of grating vector, i.e., $\Delta\beta=0$, whereas in the direction perpendicular to the grating vector, the mismatch $\Delta\alpha$ can be compensated by the mode expansion and Fourier transform of the diffracted wave for the effective interaction depth. By controlling

the interaction depth, we numerically optimize the coupling efficiency of the EO grating, and the expected experomental results are obtained.

9. REFERENCES

1. R. T. Chen, H. Lu, D. Robinson, and T. Jannson, "Highly multiplexed graded-index polymer waveguide hologram for near-infrared eight-channel wavelength division demultiplexing," Appl. Phys. Lett. **59**(10), 1144-1146 (1991).
2. R. T. Chen, H. Lu, D. Robinson, M. Wang, G. Savant, and T. Jannson, "Guided-wave planar optical interconnects using highly multiplexed polymer waveguide holograms," IEEE J. LW Tech. **10**(7), 888-897 (1992).
3. G. A. Rakuljic, V. Leyva, and A. Yariv, "Optical data storage by using orthogonal wavelength-multiplexed volume holograms," Opt. Lett. **17**, 1471-1473 (1992).
4. R. T. Chen, "Reconfigurable optical interconnection network for multimode optical fiber sensor arrays", Opt. Eng. 31(5), 1098-1106 (1992).
5. R. T. Chen, M. R. Wang, G. J. Sonek, and T. Jannson, "Optical interconnection using polymer microstructure waveguides," *Opt. Eng.* **30**(5), 622-628 (1990).
6. R. T. Chen, M. R. Wang, and T. Jannson, "Intraplane guided wave massive fanout optical interconnections," *Appl. Phys. Lett.* **57**(20), 2071-2073 (1990).
7. A. Neyer, "Electro-optic X-switch using single mode Titanium Lithium Niobate channel waveguides," *Electro. Lett.* **19**(14), 553-554 (1993).
8. C. S. Tsai, S. Kim, and F. R. El-Akkari, "Optical channel waveguide switch and coupler using total internal reflection," *IEEE J. Quantum Electron.* **QE-14**(7), 513-517 (1978).
9. R. V. Schmidt and P. S. Cross, "Efficient optical waveguide switch amplitude/modulator," *Opt. Lett.* 2, **45** (1978).
10. R. T. Chen, H. Lu, D. Robinson, Z. Sun, and J. Jannson, "60 GHz board-to-board interconnection using polymer optical buses in conjunction with microprizm couplers," *Appl. Phys. Lett.* **60**(5), 536-538 (1992).
11. A. Yariv and P. Yeh, Optical Waves in Crystals, John Wiley Sons, Inc. New York, 1984.
12. P. Moon and D. E. Spencer, Field Theory Handbook, Spinger-Verlag, Berlin, 1971.
13. K. Koshiba, Optical Waveguide Theory by the Finite Element Method, KTK Science Pulishers, Tokyo, 162-166(1992).
14. M. Li and S. J. Sheard, "Waveguide couplers using parallelogramic-shaped blazed gratings," *Opt. Commun.* **109**, 239-245 (1994).